SERBIAN JOURNAL OF ELECTRICAL ENGINEERING
Vol. 18, No. 3, October 2021, 333-349

UDC: 621.313.13 -713:004.514 **DOI: https://doi.org/10.2298/SJEE2103333V**

Experimental Study and Thermal Analysis of Cooling Systems for Brushless Motors with Double Stator and Axial Gap

Boris Georgiev Velev[1], Ivan Stoyanov Ivanov[2], Vladimir Vasilev Kamenov[3]

Abstract: The results of experimental research and thermal analysis of several types of cooling of brushless electric motors with nominal power 10-12kW (PMAC), suitable for "light" EV/HEV vehicles are presented in the research paper. The studied motors have permanent magnets, a double stator and an axial magnetic flux with air or liquid cooling. The Motor-CAD software performed the presented thermal analysis. The experimental study was made on the basis of precision results, obtained from the measurement of process temperatures during operation in a real-world environment. For this purpose, the electric motors were equipped with a number of thermocouples with which the temperatures are measured. The precise measurement and recording of the heat flux temperatures is performed using LabVIEW software. The calculations from the thermal analysis coincide with the experimental results and can be used to predict the heat fluxes in different designs and types of cooling systems. The possibilities for improving the cooling and power of standard PMAC electric motors with double stators have been studied and analyzed.

Keywords: Thermal analysis, EV/HEV – electric and hybrid vehicles, PMAC – brushless electric motor with permanent magnets, GUI – graphical user interface.

1 Introduction

At present, the design of compact brushless traction motors of the "pancake" type, with permanent magnets and axial magnetic flux (PMAC), which are up to 75% smaller than the size of conventional electric motors, and are suitable for "light" EV/HEV applications is actively developed [4, 5, 11]. Such a large percentage of size and weight reduction is due to a combination of factors, including improved classes of permanent magnets, new materials and modern manufacturing techniques. Thermal analysis and modelling are also of great importance for achieving good operating parameters and improved design

[1]Institute of Mechanics - BAS, Sofia, Bulgaria; E-mail: boris_velev81@abv.bg
[2]University of National and World Economy, Sofia, Bulgaria; E-mail: ivanov_i_s@abv.bg
[3]Technical University, Sofia, Bulgaria; E-mail: vladokamenov@gmail.com

capabilities of these electric motors [1, 2, 5 – 8]. In them, the rotor disk has a purely structural purpose, i.e. to maintain permanent magnets. The thermal paths for cooling the rotor are realized by convection through the air gap between the rotor and the stators and heat transfer to the motor shaft [5]. The general thermal paths for conduction and convection in this type of electric motors are more complex and the external convection of heat transfer depends on the level of external cooling, which can be air-cooled, liquid-cooled or combined [5, 6]. In the presented analysis, it is assumed that there is a certain level of external cooling, which leads to a fixed temperature of the housing. This assumption is not true for some PMAC motors – for example, the forced air-cooling shown in Fig. 2a and the one-sided liquid-cooling shown in Fig. 2b. Improved stator cooling can increase the efficiency and power of this type of electric motors. For this purpose, it is necessary to study and analyze the thermal paths of several types of cooling systems through both experimental tests and thermal analysis.

2 Purpose of the Work

The presented work aims to study and analyze the possibilities for improving the cooling and power of standard PMAC electric motors with double stator.

To make a comparative thermal analysis of the heat fluxes in different designs and types of cooling systems by conducting both experimental tests and thermal modelling of the cooling system of the stators, windings and housing of this type of electric motors.

To propose an improved design of the cooling system of a low-cost electric motor used in subcompact urban EV/HEV vehicles, based on the research.

The novelty of this study is that, in order to obtain reliable results, experimental tests are performed under real operating conditions in urban environments. This approach promises to be faster and more cost-effective than conventional test methods.

3 Electric motors, Means and Methods of Research

3.1 Electric motors for research

Selection of electric motors

While induction motors are a possible option for all electric vehicles (EV), limited mounting space, increased power conversion efficiency requirements and the mass/power ratio of hybrid vehicles (HEV) favor the application of brushless electric motors with permanent magnets (PMAC) [11, 12].

PMAC motors with a trapezoidal rotating magnetic field are called brushless DC electric motors (BLDC), while sinusoidal rotating magnetic field motors are called permanent magnet synchronous motors (PMSM).

The PMAC electric motors, that were studied and analyzed in the presented work, contain permanent magnets, double stator and axial magnetic flux (shown in **Table 1**). They were chosen because of their best price/performance ratio [9, 10]. According to the additional data obtained from the manufacturer [9] and EU standard IEC60034-5/2020, it can be assumed that the motors belong to the thermal class B.

Table 1

Main characteristics of PMAC electric motors with double stator.

Brand, model, type / Characteristics	Golden motor, HPM-10KW, BLDC	Golden motor, HPM-10KW, BLDC	Motenergy, ME1304, PMSM
Voltage	96 V	96 V	96 V
Rated power	8-10 kW	10 kW	14,5 kW
Efficiency	91%	91%	90%
Rated RPM	4000 rpm	4000 rpm	5000 rpm
Number of magnets	8 pcs., 4 poles	8 pcs., 4 poles	8 pcs., 4 poles
Rotor sensors	Hall sensors	Hall sensors	Sin/Cos encoder
Stators	3-phase, double, Y-connected	3-phase, double, Y-connected	3-phase, double, Y-connected
Rated torque	50 Nm	50 Nm	50 Nm
Max. temperature	No data	No data	140 ^{0}C
Cooling	Air cooled, one-sided with fan	Liquid, one-sided with glycol	Liquid, two-sided with glycol
Weight	17 kg	17,7 kg	16,5 kg
Housing	Aluminum	Aluminum	Aluminum
Length	170 mm	170 mm	170 mm
Diameter	206 mm	206 mm	206 mm
General characteristics	Sealed ribbed housing	Sealed ribbed housing	Sealed ribbed housing
Price	795$	795$	1350$

Comparative analysis of the selected electric motors

Table 1 shows the main characteristics of the selected electric motors. It is obvious that the most suitable in terms of price/weight/torque ratio are the two BLDC type electric motors model HPM-10KW, manufactured by Golden Motor Company, utilizing either air-cooling with a fan, or one-sided liquid cooling of the left stator [9]. The rated power of these electric motors is ~10 kW. The company does not offer an electric motor with a similar design, weight and geometry with double-sided liquid cooling.

The electric motor model ME1304 manufactured by the Motenergy company, which has a similar weight and geometry, has double-sided liquid

cooling and a rated power of 14.5 kW, but its price is almost twice as high, i.e. it is not a low-cost solution [10].

In order to carry out the presented research, it is necessary to calculate the required power of electric motors applicable in subcompact urban electric vehicles, which have recently become very popular [14]. In order to calculate the required power of the electric motor, it is assumed that the mass of the empty vehicle is $M = 650$ kg and the maximum mass is $M_{max} = 1000$ kg. The total power of an electric motor for driving a vehicle with a similar mass, with a certain speed and gradient of the road is selected according to the graph shown in Fig. 1 and according to the calculations presented in [13].

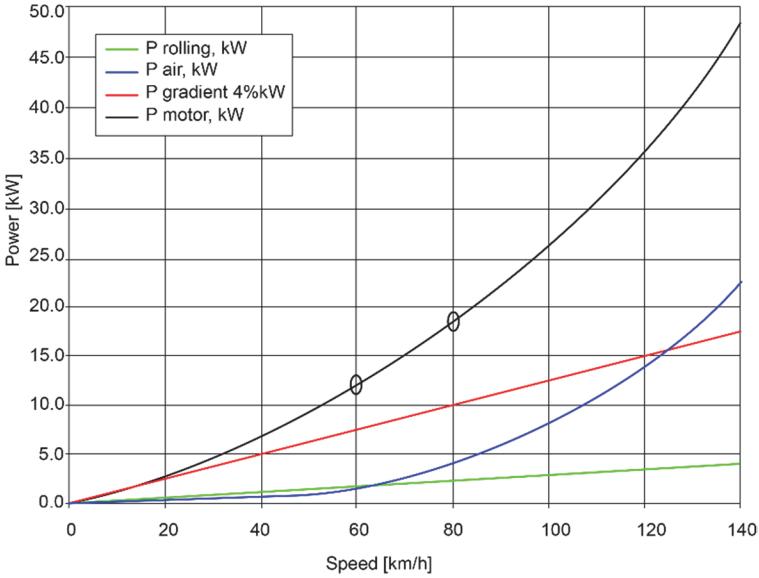

Fig. 1 – *Power requirements of the electric motor depending on the speed of the selected vehicle when climbing a* 4% *gradient.*

The graph in Fig. 1 shows the requirements for the power of the motor when overcoming a road gradient of 4% (red line), the required power when overcoming the rolling friction resistance (green line), the required power to overcome the air resistance (blue line) and the total required power (black line) of the motor depending on the speed of the vehicle.

On the curve for the required total power of the electric motor, the requirements for the power of the electric drive in urban conditions at an average speed of 60 km/h and a maximum speed of 80km/h are marked with circles. All calculations are performed with a maximum mass $M_{max} = 1000$ kg. In order to achieve a speed of 80 km/h while overcoming a 4% road gradient, the required power of the electric motor, according to Fig. 1, is:

$$P_{mot}(4\%, 80\ \text{km/h}) \approx 15\,\text{kW}\ .$$

In the same way, the required power when driving at rated speed in urban conditions at a speed of 60 km/h is determined:

$$P_{mot}(4\%, 60\ \text{km/h}) \approx 12\,\text{kW}\ .$$

The two HPM-10KW electric motors with air and liquid one-sided cooling, whose main specifications are presented in **Table 1**, were selected for experimental research.

However, calculations show that the rated power of these electric motors will not be sufficient for use in the smallest EV/HEV class of urban vehicles. Therefore, in order to increase the rated power, it is necessary, through both experimental research and thermal analysis, to offer the possibility for an improved design of the cooling system of these BLDC type electric motors shown in **Table 1** [9].

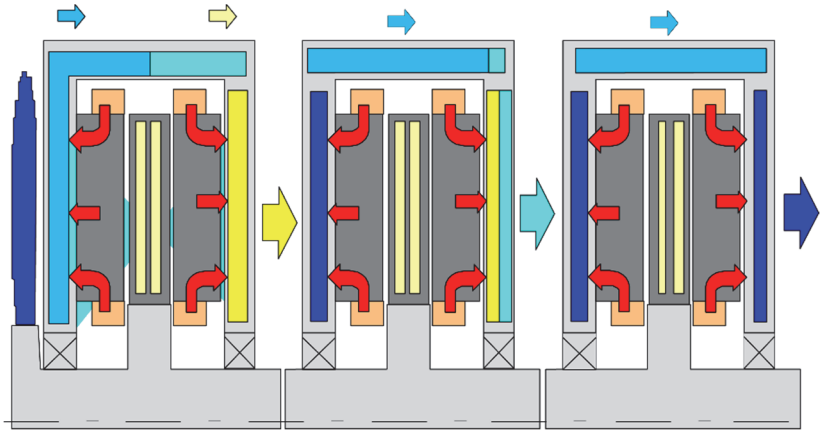

Fig. 2 – *Diagrams of three types of cooling systems, showing the thermal paths from the stators to the motor housing:*
(a) *electric motor with forced air-cooling by a fan;*
(b) *electric motor with one-sided liquid cooling;*
(c) *electric motor with double-sided liquid cooling.*

To optimize BLDC motors, it is necessary to change their cooling system from one-sided to two-sided liquid cooling. For this purpose, an additional cooling jacket is added, and an additional ring of copper pipe is mounted to the electric motor with liquid one-sided cooling, pressed to the right flange with thermally conductive paste, so that when connecting the cooling system in a certain way, an electric motor with double-sided liquid cooling is obtained, according to the scheme of Fig. 2c.

Thus, three comparable sets of BLDC electric motors with different cooling systems were prepared for testing, the axial cross sections of which are shown in Fig. 2, respectively: (a) – electric motor with forced air cooling by a fan; (b) – electric motor with forced liquid cooling only on the left side and (c) – electric motor with forced liquid cooling on both sides. The red arrows of the diagrams indicate intensive thermal transfer from the stators and windings to the cooling flanges and the housing, the blue arrows indicate good thermal conductivity of the cooling of the housing, and the yellow arrows indicate poor thermal conductivity of the cooling of the housing. Wide arrows denote the degree of cooling of the housing by convection, and their colors characterize the cooling by thermal transfer from the flanges to the housing: dark blue - very good cooling; light blue - good cooling and yellow - poor cooling.

3.2 Experimental setup

The electric motors were tested on an experimental setup, installed in a test vehicle, equipped with a mechatronic system for real-time testing and monitoring of lithium-ion batteries, transmissions and traction motors intended for EV/HEV vehicles [3]. It consists of two main mechatronic modules – *electro-mechanical module and electronic module.*

The electro-mechanical module is the main module of the system and consists of the following main components: traction batteries; traction motors and mechanical components. The mechanical components are selected among standard automotive parts in order to simplify the stress calculations in the design stage and reduce the cost of the system. They consist of differential; geared, belt or chain drive; clutch and wheels (Fig. 3b). All of these components can work together with the electric motor and the battery as a stand-alone module, or as a mechatronic module in the mechatronic test system, in different configurations. The configuration and size of the components shall be such as to permit installation of the system in a test vehicle, which will be able to perform the required tests in a real environment. The electromechanical module is connected to the rear running gear of the test vehicle. Fig. 3a shows the layout and Fig. 3b the block diagram of the electromechanical module, where the thermal transfer of a mounted electric motor (3) with forced air-cooling by an axial fan is shown in colors.

The electronic module consists of a battery management system (BMS), sensors and actuators, an interface for communication between the systems and a computer for processing and evaluating experimental data. The system is equipped with a graphical interface (GUI) for recording and analyzing experimental data from many process parameters. The computer, in turn, is connected through a suitable interface to other components of the system, such as the motor controller, the charger and the LabVIEW software. Fig. 4 shows the diagram of a part of the cooling system of the test vehicle's internal combustion

engine (ICE), to which the cooling system of the electric motors is connected, as well as the components of the mechatronic module, necessary for the thermal tests.

(a)

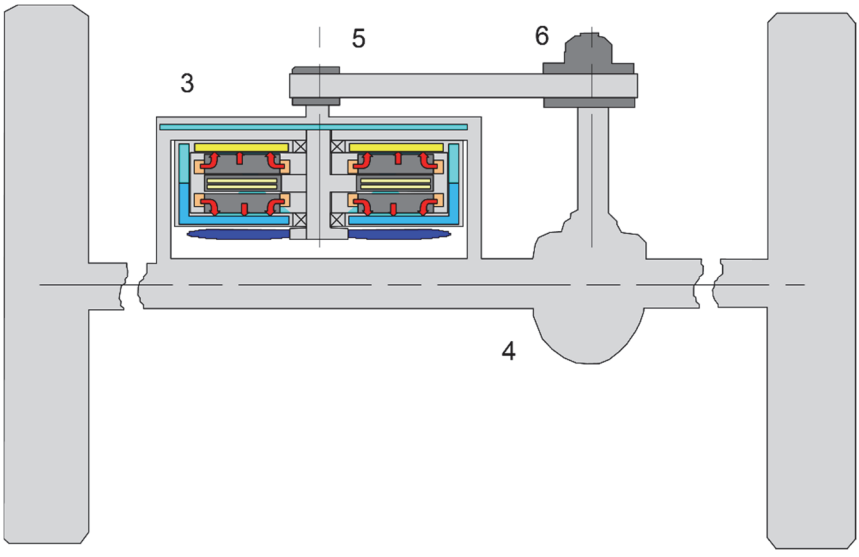

(b)

Fig. 3 – *Electromechanical module of the mechatronic test system in real test conditions:* (a) *Picture of the module in the test vehicle;*
(b) *Block diagram of the module: 1- charger, 2 - controller, 3 - electric motor, 4 - differential axle with wheels, 5 - belt drive, 6 - clutch.*

The cooling system of the test setup works as follows: when testing an electric motor with forced air cooling, by closing the valve (7) and switching off the centrifugal pump (8), the flow of glycol to the cooling system is stopped, because the valve (14) prevents the entry of coolant from the ICE cooling system (11). At the beginning of the tests, the air-cooled electric motor (Fig. 2a) is mounted on the differential axle and the test begins. After completion of the tests, it is removed and an electric motor with one-sided liquid cooling is installed in its place (Fig. 2b). By switching on the centrifugal pump (8) the pressure in the cooling system rises and the glycol passes through the cooling jacket of the left motor flange through the valve (14) and enters the radiator (9) of the engine cooling system for cooling (it is shown in Fig. 4 in a simplified form for clarity). Then the test begins. After completing the test, the valve (7) opens and the copper coil (6), which is firmly pressed to the right motor flange by means of an aluminum plate attached to the differential housing, is filled with glycol. In this way, the test of an electric motor, which now has a liquid-cooled cooling system on both stators, according to Fig. 2c can begin.

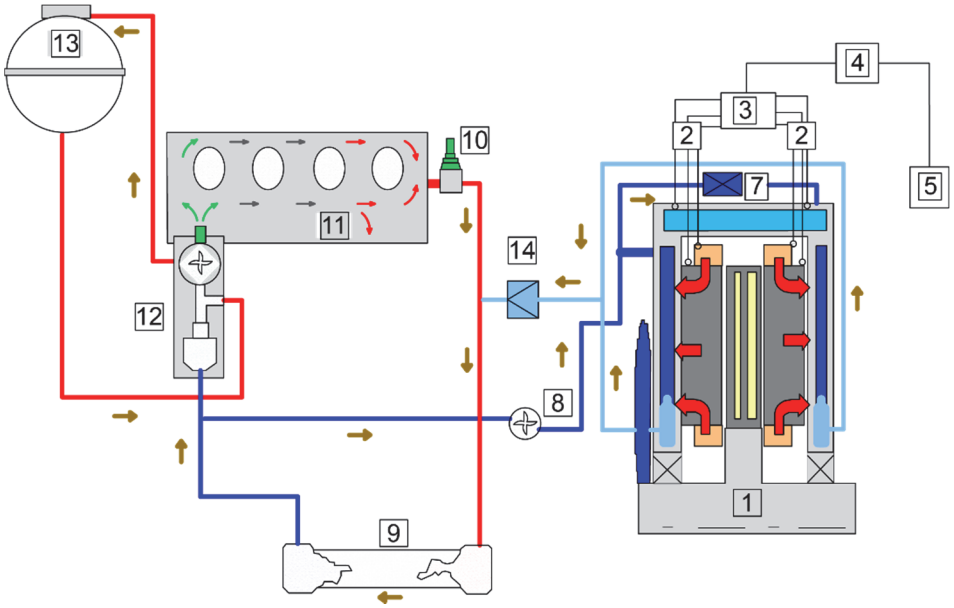

Fig. 4 – *Diagram of the cooling system and part of the mechatronic module.*

Fig. 4 shows:

1. combined scheme of the tested electric motors;
2. thermocouples;
3. amplifier;
4. data logger module (USB-DAQ Labjack-U3);

5. laptop;
6. copper serpentine coil;
7. valve;
8. centrifugal pump;
9. radiator;
10. temperature sensor;
11. internal combustion engine (ICE);
12. thermostat and centrifugal pump from the ICE;
13. expansion vessel;
14. valve.

3.3 Research and analysis methods

Methods for thermal analysis

The authors of [5] studied thermal modelling of a similar PMAC electric motor with a rated power of 10 kW, but they used a complex three-dimensional model created in the PORTUNUS simulation software package [15]. In their thermal analysis, it is assumed that the rear parts of the stators are firmly connected to the end flanges of the housing and the heat generated in them is dissipated symmetrically by convection when using air-cooling or by thermal transfer when using liquid cooling. The thermal analysis in the cited article focuses only on predicting the internal conductive and convective thermal transfer through the air gap. In order to simplify the model, the authors used only half of the motor, due to the symmetry along the axial length.

In the cases presented in the current research, such simplification is not possible because some of the motors are cooled by one-sided forced air or liquid cooling on one side only (left stator only), as shown in Fig. 2a and 2b, and thermal transfer paths are not symmetrical. Therefore, we assume that the thermal transfer and convection from the rotor disk with the magnets to the shaft and stators is constant and symmetrical, as in [5], but the convection and thermal transfer paths of the stator packages and windings to the motor housing differ (Fig. 2). Therefore, only the external paths of conductive thermal transfer and convection thermal transfer should be predicted, because the electric motors are mounted directly on the rear axle in the suspension mass of the test vehicle in real operating conditions, where the incoming airflow blows and cools them while driving. Only the approach of system calibration has been adopted from the authors of [5].

For thermal analysis in the presented work, a thermal model from the BPM-Therm module database of Motor-CAD software designed for thermal modelling of brushless electric motors with permanent magnets (BPM) [16], was chosen. This software for thermal modelling of electric motors provides a fast and accurate method for analysis and optimization of cooling systems, fully taking

into account the thermal aspects [1, 2, 4, 16]. The prediction nods are automatically placed at important points in the cross section of the motor, such as between the flanges and the iron of the stator, the windings and the stator and others. They are connected by conductivity, convection and irradiative thermal resistances, which are introduced automatically. An analysis of the liquid-cooling system, aiming to calculate the pressure drop and predict the flow rates, has already been done in [1, 2, 4] and is not considered in the presented work. A complete description of the electromagnetic design of such electric motors has also already been presented in [2], so here only the main parameters that are introduced in the simplified thermal model using BPM-Therm software analysis module are given:

– Electromagnetic parameters for evaluation of PM motor with double stator: Rated power 10 kW; Rated torque 50 Nm; Rated speed during testing 3000 rpm; Rated voltage of a phase of the rotating magnetic field 96 V; Rated current 40 A; Rated frequency of the inverter 133 Hz.
– Geometric parameters: Number of pole pairs 4; Number of slots 8; Outer active radius 170mm; Inner active radius 120 mm; End connection outer radius 197 mm; Stator yoke thickness 11mm; Slot width 14 mm; Slot height 14 mm; Conductor size 6.3×1mm (6.085 mm^2); Slot filling coefficient 0.78; Wedge thickness 2.5 mm; Average width of the magnet 45 mm; Total thickness of the magnet 3×5 mm; Total mechanical air gap 2.5×2 mm.

These and some other necessary additional parameters - axial section of the machine, cooling fins of the housing, seals between the components, insulation, etc., are imported in the simulation module BPM-Therm for predicting the thermal transfer paths. MS Excel is used to calculate the parameters required for the model and to automatically load this data into the simulation as a user interface before and after processing. The analysis focuses on predicting the internal conductive thermal transfer through the silicon steel package of the stators, firmly connected to the end flanges and the housing, which are ribbed and serve as radiators. Through them, the heat generated in the stators is dissipated by forced cooling (air or liquid, by a fan or cooling jackets in the flanges, firmly connected to the housing).

Of course, this simplified thermal modelling does not give a detailed picture of thermal paths under dynamic loads – for example, in urban driving at variable speeds, in variable operating modes, with recuperation on, etc., but it is enough to analyze the possibilities for improving the cooling and the power of standard PMAC motors. A combined electromagnetic and thermal 3D model with a volume circuit of this type of electric motors will be the subject of a subsequent project, when based on current research and after making the proposed design improvements, the possibility of increasing the rated power is clarified.

Methods for experimental research

To perform the experimental tests using the electromechanical module, the two variants of BLDC motors from **Table 1** are installed one after the other, and the valve (7) from the diagram of Fig. 4 is opened to simulate a motor with double-sided liquid cooling. Temperature measurement is performed by thermocouples installed in the selected for analysis assemblies of the electric motors during operation. The temperatures from the thermocouples are recorded continuously with accuracy $T \approx \pm 0.5°\mathrm{C}$ at nominal motor speeds of ~3000rpm and a certain torque of ~30 Nm. In general, 2×3 K-type thermocouples are mounted in different assemblies – 3 on the upper left half and 3 on the upper right half of the motors, numbered according to Fig. 5. The signals from them, according to the scheme of Fig. 4, through the MAX31850K type amplifier used for thermocouples and an interface 1-Wire (3), are fed to the data acquisition module USB-DAQ Labjack-U3 (4) and are saved via the GUI of the LabVIEW software on the computer (5), where the data from the graphics are transferred automatically to Excel for comparative analysis and evaluation, according to a specially developed software using the following algorithm:

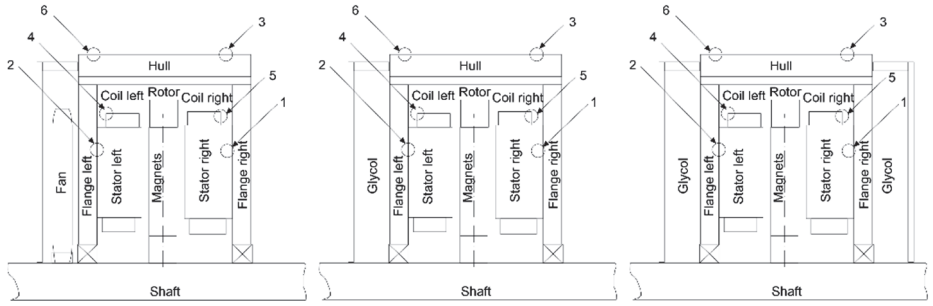

Fig. 5 – *Location of the thermocouples in the electric motors having three types of cooling;* (a) *one-sided air cooling;* (b) *one-sided liquid cooling;* (c) *double-sided liquid cooling.*

The obtained online data from the temperature vs. time graph in the respective assembly $T_{exp} = F(t)$ from the LabVIEW software is approximated with functions of the form:

$$T_{exp} = a_k \exp\left\{ b_k \left[\exp(c_k t)\right]\right\}, \tag{1}$$

where: a_k, b_k, c_k are coefficients of proportionality based on empirical data, which are selected so that the shape of the approximated curve is as close as possible to that calculated by the software module BPM - Therm. In the case of calibration: $a_k = 85$, $b_k = -0.652$, $c_k = -0.08$.

These dependences are approximated by the nonlinear equation:

$$T_{exp}[\varphi_l(t^{(1)})] - A_{exp}[\varphi_l(t^{(2)})] = 0\,. \quad (2)$$

Equation (2) determines the maximum value of T_{exp} between the values of the approximated data from the experimental tests, when the cooling enters equilibrium, i.e. when the temperature of the analyzed assembly remains constant over time. This determines the time at which the beginning of the equilibrium temperature $T_{exp} = T_e$ begins.

The graph of the calculated data for the respective assembly is similarly approximated by an equation of the type (2), where the maximum value of T_{calc} is determined, at which the values of the calculated data are constant. The graphs of the experimental and calculated data are compared automatically. If the difference between them exceeds 3–4%, correction of some of the parameters imported in the thermal model BPM-Therm is necessary, while $T_{calc} = T_e \sim 3$–4%. The tests are performed for the time at which T_e is reached for all tested assemblies. Thus the calibration of the system is completed and the experimental tests can begin. Fig. 6 illustrates the procedure for calibrating the air-cooled motor assembly: left flange/left stator, where the rear of the stator is firmly connected to the left flange (Fig. 5a). The left flange is cooled by a fan and the heat generated in the stator is dissipated by forced ventilation.

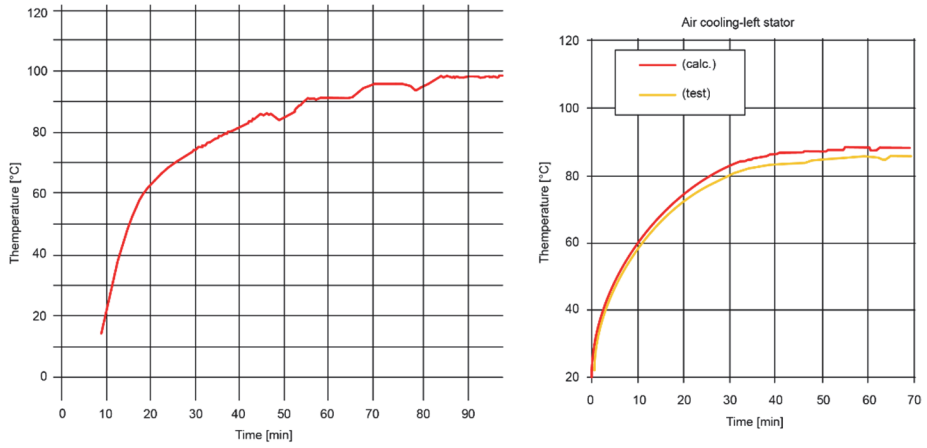

(a) (b)

Fig. 6 – *Comparison of measurements and calculations obtained from the graphs of temperature vs. time, when calibrating a single assembly of an air-cooled BLDC motor:*
(a) *Online graph of temperature vs. time: $T = F(t)$ in the corresponding assembly in LabVIEW;*
(b) *Comparative analysis and evaluation of $T_{calc} = T_e$ in MS Excel.*

All elements have selected values from the BPM-Therm database and are imported into the thermal model for calculation of temperature dependences on time.

4 Experimental Studies

The liquid of the cooling system is glycol (antifreeze) with an initial temperature of 20°C and a final temperature of not more than 80°C when the equilibrium temperature T_e of the system is reached. The initial ambient temperature is also 20°C. The air flow rate through the fan is initially assumed to be 138 m^3/h at 3000 rpm, and the coolant flow rate is constant ~8 l/min, at a pressure of 1.5 bar. During the tests, the internal combustion engine does not operate, recuperation is also switched off.

4.1 Calibration of experimental studies and thermal modelling

The first series of experiments was performed in order to calibrate the system in stationary conditions. The test vehicle is placed on a brake systems test bench, which is adjusted with such braking force on the rear pair of wheels that the current supply to the motor is ~40 A for 60 min (heavy mode operation). These tests allow the weaknesses in the thermal model to be determined and corrected experimentally, while the differences between the experimental measurements and the calculated values of temperatures do not exceed 3–4%. The calibration procedure is performed according to the example on Fig. 6 of the methods described above, for all selected assemblies in the motors.

4.2 Experimental tests in a real environment

The experimental tests in real environment are carried out after the calibration of the system, in real conditions on an asphalt section of the road with partial overcoming of the road gradient up to 4%, on average up to 40 km/h for 60 min in dry weather. The electric motor operates in heavy mode with an average supply current of 40 A, with an average speed of 3000 rpm with a fully charged traction battery pack at the beginning of each test. At the beginning of each test, it is checked that all operating parameters of the assemblies are the same and correspond to the desired configurations in terms of: ambient temperature, coolant temperature, motor load, rotor speed and others. Each test is performed three times under the same conditions. Mean test values are taken to correct nonconformities.

5 Results of Experimental Research and Thermal Analysis

Fig. 6a presents the online graph from LabVIEW software for calibration of experimental data on temperature versus time: $T_{exp} = F(t)$ in the assembly: left stator/left flange. Fig. 6b shows the two graphs of temperature vs. time: $T_{exp} = F(t)$

and $T_{calc}=F(t)$, when calibrating the predicted and experimental data in MS Excel, after approximation according to (1) and (2) of the algorithm presented above. In this case, in order to reduce the maximum value of T_{calc} to reach $T_{calc}=T_e \sim 3–4\%$, it is necessary to increase the imported value of air flow rate from Q = 138 m^3/h to Q =240m^3/h of forced fan cooling in BPM-Therm module. Fig. 7a shows a match between the experimental and calculated transient temperatures inside the assembly at the rear of the left stator/left flange of the forced air-cooled motor, initially calibrated according to the methods described above. However, even in the first experimental tests in a real environment, a large difference was observed between the predicted and experimental results of the temperatures at the right stator of this electric motor.

The experimental temperatures in the real-world tests are lower than the experimental temperatures in the calibration of the same assembly. Apparently, the calibration procedure failed to take into account the convection to the right end of the housing from the forced blowing of outside air when moving in a real environment. The other components of the assemblies for simulating the conducted thermal transfer must be the same i.e. cannot be corrected in the thermal model. Therefore, in order to be accurate in the predicted results, we must additionally introduce in the calibration procedure a coefficient of convection of the air blowing to the right-stator/right-flange assembly. Fig. 7b shows in solid red lines the calculated results of the second calibration for the right stator of this motor, which almost coincide with the experimental results in real conditions. Fig. 8 shows the graphs of the experimental and predicted results of the temperatures in the air-cooled electric motor.

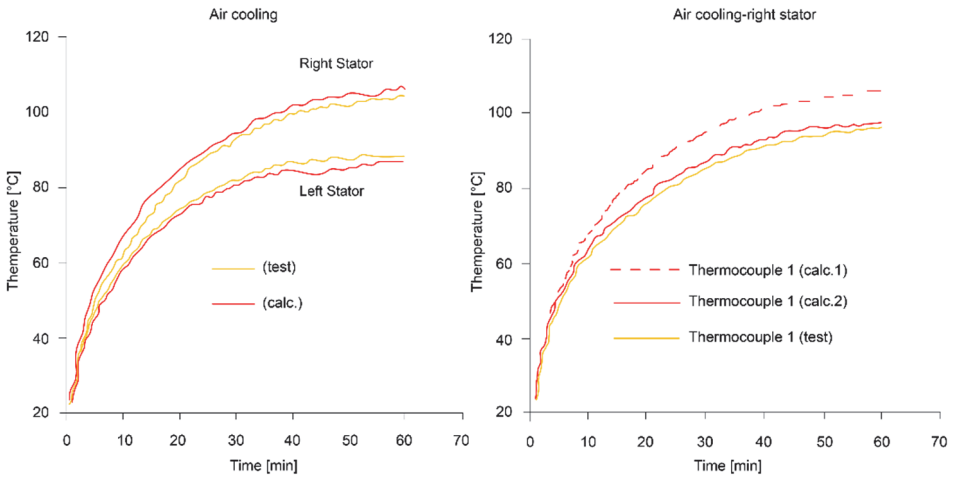

(a) (b)

Fig. 7 – *Calibration test of assembly temperature – stators/flanges when using air cooling:* (a) *left stator;* (b) *right stator.*

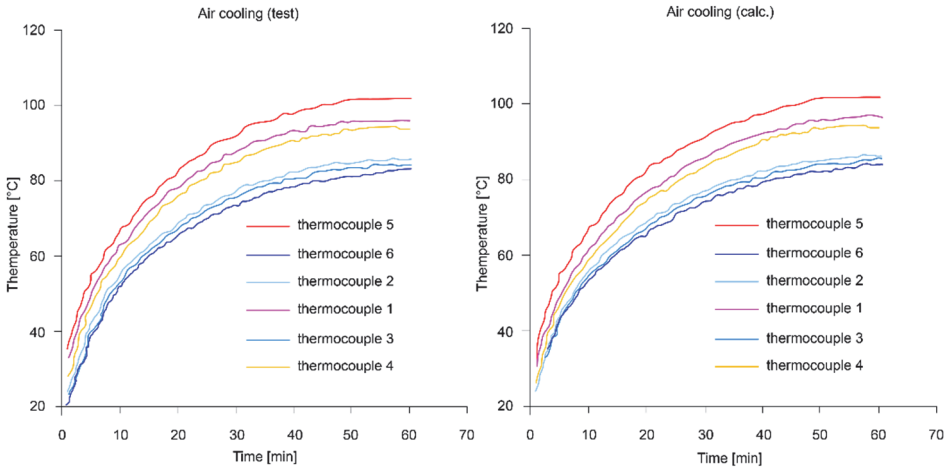

Fig. 8 – *Graphs of experimental and predicted temperature results for air-cooled electric motors;* (a) *experimental results;* (b) *predicted results.*

The graphs of the results of the calculated and experimental temperatures from the calibration tests in the cases of one-sided and two-sided liquid cooling coincide with a difference of up to 3–4%, which is within acceptable limits. As only the values of the final equilibrium predicted and experimental temperatures are important for the comparative analysis, instead of graphically presenting all the graphs, the data from them are shown in **Table 2**, where these temperatures are directly compared to better estimate how the thermal model fits the experiments for each type of cooling. The table summarizes the numbers in order, the color of the curves and the final predicted and experimental equilibrium temperatures for each studied motor assembly. It is obvious that the temperature decrease on the right side of the stator is only 2°C compared between one-sided cooling and two-sided cooling, which is probably caused by one of the thermocouples bad contact. However, the tendency of the temperature to decrease is evident and it is correct to leave the true value without adjusting it.

Table 2 also shows that the calculated temperatures for the right end of the housing and the right stator in the one-sided liquid cooling, Fig. 5b are higher than the experimental ones by about 6–7%, while in the calibration they almost coincide. Therefore, the experimental temperatures for one-sided liquid cooling are not the same in the stationary calibration test and the real road test. Probably the difference is due to some convection from the airflow when driving on the road, because the electric motor is located in the sub-spring mass of the test vehicle, as shown in Fig. 3. These differences are within acceptable limits and are considered negligible, and in this case, unlike the case of one-sided air-cooling,

there is no need for additional adjustment of the model. In the variant with double-sided liquid cooling, Fig. 5c, the predicted and experimental results almost coincide.

Table 2
Location of thermocouples, colour of curves and final predicted and experimental equilibrium temperatures T_e.

No. from Fig. 5	Colour of the curves from Fig. 8	Location of thermocouples from Fig. 5	Air cooling [°C]		One-sided liquid cooling [°C]		Double-sided liquid cooling [°C]	
			T_{est}	T_{calc}	T_{est}	T_{calc}	T_{est}	T_{calc}
2.	light blue	stator left	84.5	84	81.5	82.5	82	82.5
4.	dark yellow	coil left	94	92.5	90.5	92	90.5	90
6.	dark blue	housing left side	82.5	82	80.5	82	80	80.5
3.	blue	housing right side	84	84.5	81	83.5	80	80.5
5.	red	coil right	102.5	100	91.5	92.5	90	90.5
1.	light red	stator right	95.5	95	84.5	85.5	82	82.5

6 Conclusion

In the comparative thermal analysis of the experimental and predicted results of temperatures in the main assemblies of thermal paths in different designs and types of cooling systems, the possibility of improving the cooling and power of low-budget PMAC dual stator motors suitable for sub-compact urban EV/HEV vehicles is proven.

Based on the research, an improved design of the cooling system has been proposed, as it can be converted from one-sided liquid cooling of only one stator to two-sided liquid cooling of both stators.

The errors in the predicted and experimental results of the research are in the range of 3–4% and reach a maximum of 6–7%, therefore the results can be considered a very good match. The proposed model is able to predict thermal transitions with a maximum error below 7% and can easily be used to accurately predict the heat fluxes for different types of cooling of this type of electric motors.

7 Acknowledgment

This work was implemented under project M27/7 from 2018, funded by the Research Fund of the Ministry of Education and Science.

8 References

[1] D.A. Staton: Permanent Magnet Motor CAD: Thermal Design Aspects, The UK Magnetics Society Seminar – Developments in the Manufacture and Use of Permanent Magnets, Austin Court, Birmingham, UK, November 2000, pp. 1 – 6.

[2] D.G. Dorrell, D.A. Staton, M.I. McGlip: A Combined Electromagnetic and Thermal Approach to the Design of Electrical Machines, Proceedings of the 32nd Annual Conference on IEEE Industrial Electronics (IECON 2006), Paris, France, November 2006, pp. 1 – 6.

[3] B. Velev, B. Banov, G. Velev: System for Testing of Lithium-Ion Batteries and Electric Motors for Electrical Vehicles, Proceedings of the 20th International Scientific and Technical Conference on Transport, Road-Building, Agricultural, Hoisting & Hauling and Military Technics and Technologies (trans&MOTAUTO'12), Varna, Bulgaria, June 2012, pp. 79 – 82.

[4] D. Staton, D. Hawkins, M. Popescu: Practical Strategies for Improved Cooling of Electrical Motors and Generators, Motor Design Ltd., Ellesmere, Shropshire, UK, pp. 1 – 8.

[5] Gy. Vainel, D. A. Staton, F. G. Capponi, G. De Donato, F. Caricchi: Thermal Modelling of a Fractional-Slot Concentrated-Winding Kaman Type, Axial-Flux Permanent-Magnet Machine, Proceedings of the IEEE Energy Conversion Congress and Exposition, Denver, Co, USA, September 2013, pp. 1505 – 1511.

[6] T. Davin, J. Pellé, S. Harmand, R. Yu: Experimental Study of Oil Cooling Systems for Electric Motors, Applied Thermal Engineering, Vol. 75, January 2015, pp. 1 – 13.

[7] Y. Yang, B. Bilgin, M. Kasprzak, Sh. Nalakath, H. Sadek, M. Preindl, J. Cotton, N. Schofield, A. Emadi: Thermal Management of Electric Machines, IET Electrical Systems in Transportation, Vol. 7, No. 2, June 2017, pp. 104 – 116.

[8] L. Frosini, M. Malinverni, M. Cima, N. Anglani: Thermal and Electromagnetic Modelling for Prototyping Permanent Magnet DC Motors, Proceedings of the XIII International Conference on Electrical Machines (ICEM), Alexandroupoli, Greece, September 2018, pp. 1330 – 1337.

[9] Golden Motor, Available at: https://www.goldenmotor.com/

[10] Motenergy, Available at: http://www.motenergy.com

[11] All about Circuits: Brushless DC Motor, Chapter 13 - AC Motors, Available at: http://www.allaboutcircuits.com/vol_2/chpt_13/6.html

[12] S. B. Ozturk: Modelling, Simulation and Analysis of Low-Cost Direct Torque Control of PMSM Using Hall-effect Sensor, MSc Thesis, Texas A&M University, Faculty of Electrical Engineering, Bryan, 2005.

[13] D. Doerffel: Testing and Characterisation of Large High-Energy Lithium-Ion Batteries for Electric and Hybrid Electric Vehicles, Ph.D. dissertation, University of Southampton, Faculty of Engineering, Science and Mathematics, Southampton, 2007.

[14] Forbes: China's Electric Car Revolution Is Being Led By The Hongguang Mini, December 2, 2020, Available at: https://www.forbes.com/sites/jimcollins/2020/12/02/chinas-electric-car-revolution-is-being-led-by-the-hongguang-mini/

[15] Portunus v4.1, System Simulation Software: https://portunus.software.informer.com/

[16] Motor Design Limited, Available at: https://www.motor-design.com/motor-cad/